A model intercomparison of atmospheric 137Cs concentrations from the Fukushima Daiichi Nuclear Power Plant accident, phase III: Simulation with an identical source term and meteorological field at 1-km resolution

Yousuke Sato, Thomas Sekiyama, Sheng Fang, Mizuo Kajino, Arnaud Querel, Denis Quelo, Hiroaki Kondo, Hiroaki Terada, Masanao Kadowaki, Mazayuki Takigawa, et al.

ATMOSPHERIC ENVIRONMENT: X 7 (2020) 100086

Contents lists available at ScienceDirect

Atmospheric Environment: X

journal homepage: http://www.journals.elsevier.com/atmospheric-environment-x

A model intercomparison of atmospheric ^{137}Cs concentrations from the Fukushima Daiichi Nuclear Power Plant accident, phase III: Simulation with an identical source term and meteorological field at 1-km resolution

Yousuke Sato [a,*], Tsuyoshi Thomas Sekiyama [b], Sheng Fang [c], Mizuo Kajino [b], Arnaud Quérel [d], Denis Quélo [d], Hiroaki Kondo [e], Hiroaki Terada [f], Masanao Kadowaki [f], Masayuki Takigawa [g], Yu Morino [h], Junya Uchida [h], Daisuke Goto [h], Hiromi Yamazawa [i]

[a] Faculty of Science, Hokkaido University, Sapporo, Hokkaido, Japan
[b] Meteorological Research Institute, Tsukuba, Ibaraki, Japan
[c] Institute of Nuclear and New Energy Technology, Tsinghua University, Beijing, China
[d] Institut de Radioprotection et de Sûreté Nucléaire (IRSN), Fontenay-aux-Roses Cedex, France
[e] National Institute of Advanced Industrial Science and Technology, Tsukuba, Japan
[f] Japan Atomic Energy Agency, Naka-Gun, Ibaraki, Japan
[g] Japan Agency for Marine-Earth Science and Technology, Yokohama, Kanagawa, Japan
[h] National Institute for Environmental Studies, Tsukuba, Ibaraki, Japan
[i] Department of Applied Energy, Graduate School of Engineering, Nagoya University, Nagoya, Aichi, Japan

ARTICLE INFO

Keywords:
Model intercomparison project for atmospheric ^{137}Cs
Atmospheric dispersion model
Radionuclide

ABSTRACT

The third model intercomparison project (MIP) for investigating the atmospheric behavior of atmospheric caesium-137 (^{137}Cs) emitted from Fukushima Daiichi Nuclear Power Plant (FDNPP) (3rd FDNPP-MIP), Japan, in March 2011, was conducted. A finer horizontal grid spacing (1 km) was used than in the previous FDNPP-MIP (2nd FDNPP-MIP, Sato et al., 2018; 3 km) to evaluate the models' performance for high-concentration events measured near FDNPP. Nine of the models used in the 2nd FDNPP-MIP were also used in the 3rd FDNPP-MIP, and all models used identical source terms and meteorological fields. The performance of the models was evaluated through a comparison with observational data. Our analyses indicated that most of the observed high atmospheric ^{137}Cs concentrations (plumes) were reasonably well simulated by the models, and the good performance of some models improved the performance of the multimodel, highlighting the advantage of using a multimodel ensemble. The analyses also confirmed that the use of a finer grid resolution resulted in the meteorological field near FDNPP being better reproduced in the 3rd FDNPP-MIP, and the performance of the models was better than that of the 2nd FDNPP MIP. The good representation of the wind field resulted in the reasonable simulation of the narrow distribution of high deposition amount to the northwest of FDNPP and the reduction of the overestimation in deposition amount over the area to the south of FDNPP compared to the 2nd FDNPP MIP. In contrast, the performance of the models in simulating plumes observed over the Nakadori area, the northern part of Gunma, and the Tokyo Metropolitan Area (TMA) was slightly worse than in the 2nd FDNPP-MIP.

1. Introduction

Large amounts of radionuclides, including caesium-137 (^{137}Cs), were emitted to the atmosphere after the accident at Fukushima Daiichi Nuclear Power Plant (FDNPP) in Japan, which was triggered by an earthquake and seismic sea wave in March 2011. The radionuclides were widely dispersed by atmospheric advection and subsequently deposited over the land and ocean. After the accident, a number of studies investigated the behavior of the atmospheric ^{137}Cs through observations (e.g., Adachi et al., 2013; Honda et al., 2012; Igarashi et al., 2015; Kaneyasu et al., 2012; Moriizumi et al., 2019; Oura et al., 2015; Sanada et al., 2018; Science Council of Japan, 2014; Terasaka et al., 2016; Tsuruta et al., 2014, 2018) and modeling (e.g., Chino et al., 2011; Draxler et al., 2015; Hu et al., 2014; Kajino et al., 2016; Katata et al., 2012;

* Corresponding author. Faculty of Science, Hokkaido University, Kita-10, Nishi-8, Kita-ku, Sapporo, Hokkaido, 060-0810, Japan.
E-mail address: yousuke.sato@sci.hokudai.ac.jp (Y. Sato).

https://doi.org/10.1016/j.aeaoa.2020.100086
Received 17 April 2020; Received in revised form 21 July 2020; Accepted 21 July 2020
Available online 4 August 2020

Korsakissok et al., 2013; Mathieu et al., 2018; Morino et al., 2011; Stohl et al., 2012; Takemura et al., 2011; Terada et al., 2012; Yasunari et al., 2011). These studies demonstrated that modeling is a powerful tool for understanding the behavior of ^{137}Cs. However, the numerical models themselves contained uncertainties originating from various factors, e.g., input data, including the meteorological field (Arnold et al., 2015), emission inventory (source term) (Li et al., 2019; Morino et al., 2013; Nakajima et al., 2017; Saunier et al., 2013), grid resolution (Sekiyama et al., 2015), distribution of cloud and precipitation (Saito et al., 2015), modeling of the physical processes of the radionuclides (Dacre et al., 2020; Leadbetter et al., 2015; Morino et al., 2013; Quérel et al., 2015), and other factors. Due to these uncertainties, simulated atmospheric ^{137}Cs typically differed from model to model.

To understand and evaluate inter-model variation, model intercomparison is useful. Several model intercomparison projects (MIPs) have been conducted to elucidate the inter-model spread of general circulation models (e.g., Eyring et al., 2016; Huneeus et al., 2011; Meehl et al., 2000; Myhre et al., 2013; Thibeault et al., 2010), large eddy simulation models (e.g., Ackerman et al., 2009; Blossey et al., 2013; Bretherton et al., 1999; Stevens et al., 2005; VanZanten et al., 2011), chemical transport models (e.g., Bessagnet et al., 2016; Dore et al., 2015), and others. Draxler et al. (2015) conducted an MIP study of atmospheric dispersion models targeting ^{137}Cs emitted from FDNPP. Following their MIP study, our group conducted two MIPs (Kitayama et al., 2018; Sato et al., 2018). Kitayama et al. (2018) conducted an MIP to study the atmospheric ^{137}Cs emitted from FDNPP (the 1st FDNPP-MIP) using seven atmospheric dispersion models and highlighted the advantage of a multimodel ensemble for simulating atmospheric ^{137}Cs activity concentrations (henceforth we just refer to "atmospheric ^{137}Cs concentrations") and ^{137}Cs deposition. The advantage of the multimodel ensemble is "cancel out" of bad performance in some models through averaging whole models. Kitayama et al. (2018) also reported a large inter-model spread, although the reasons for this spread were unclear because each model used different source terms, horizontal and vertical grid resolution, domain size, and meteorological data. Thus, too many factors were involved to establish the reason for the inter-model variation.

Sato et al. (2018) conducted the second MIP for atmospheric ^{137}Cs (the 2nd FDNPP-MIP; henceforth referred to as the 2nd MIP) using the same meteorological data, the same emission inventory, and the same horizontal grid spacing of 3 km to minimize the differences between the models as much as possible. They evaluated 12 models by comparing the results of each model with both atmospheric ^{137}Cs measurements from the suspended particulate matter (SPM) network (Oura et al., 2015) and aircraft measurements of ^{137}Cs deposition (MEXT, 2011). Although their analyses also highlighted the advantages of using a multimodel ensemble, they did not evaluate the model performance for high-concentration events (henceforth referred to as "plumes") measured at the SPM sites near FDNPP (i.e., the Haramachi, Soma, and Shinchi sites; Fig. 1b). This was because the resolution of the model (3 km) was too coarse to evaluate its validity according to assessments of the effective resolution reported by Frehlich and Sharman (2008) and Skamarock (2004). Skamarock (2004) and Frehlich and Sharman (2008) reported that models cannot simulate phenomena with spatial scales smaller than 6–10 times the grid spacing; the distance from FDNPP to some of the sites was less than 6–10 times the grid spacing.

To overcome this problem and evaluate models' performance, an MIP with fine grid spacing is required. In this study, we conducted the 3rd FDNPP-MIP (henceforth referred to as the 3rd MIP) for atmospheric ^{137}Cs using the same emission inventory as in the 2nd MIP, finer grid resolution, and meteorological data with finer grid spacing (1 km) than in the 2nd MIP. Based on the results of the models using finer grid resolution, we evaluated their performance for simulating the plume measured over sites near FDNPP. In addition, the results of a recent observational study (Tsuruta et al., 2018) were also used in the evaluation.

In this paper, we present an overview of the 3rd MIP and an evaluation of models' performance for the plume near FDNPP. We also highlight the advancements made in the 3rd MIP relative to the 2nd MIP.

2. Material and method

2.1. Participating models and experimental setup

In both the 2nd and 3rd MIPs, of the various radionuclides emitted from FDNPP, only ^{137}Cs was targeted (Sato et al., 2018). The nine models listed in Table 1 were included in the 3rd MIP, and all of them were also included in the 2nd MIP. Except for SCALE, WRF-Chem-J and GEARN, the versions of the models used in the 3rd MIP were the same as those used in the 2nd MIP. In the time between the two projects, the dynamical cores of the GEARN and WRF-Chem-J models were updated from WRF version 3.6.1 to WRF version 4.1 and from WRF version 3.6 to WRF version 4.1.1, respectively. The SCALE components were updated as described in Table 1. The basic information for each model, such as resolution, Eulerian/Lagrangian, with/without dynamical core, reference, and other parameters are listed in Table 1. As described in Table 1, the vertical resolution was different from model to model as in the 2nd MIP. Generally speaking, the vertical resolution has large impact on the

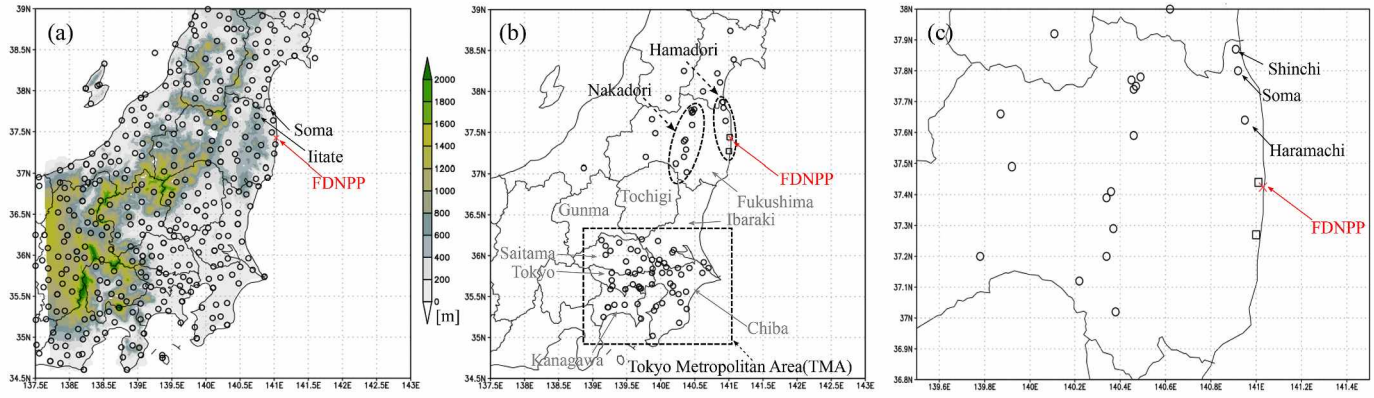

Fig. 1. Calculation domain with (a) (shaded) elevation of topography and (circle) location of the AMeDAS observation site, and (b) location of SPM observational sites used in (circle) Oura et al. (2015) and (square) Tsuruta et al. (2018). (c) Same as (b), but extended to Fukushima Prefecture. The red crosses in (a), (b), and (c) show the location of FDNPP. The names of the regions and observation sites are shown in black characters, and the names of prefectures are shown in grey characters in (b). The names of SPM sites discussed in the body of the manuscript are shown in (c). The maps in the figures were constructed using the Grid Analysis and Display System (GrADS: Institute for Global Environment and Society (IGES), 1989). (For interpretation of the references to colour in this figure legend, the reader is referred to the Web version of this article.)

Table 1
Summary of the participating models and NHM-LETKF used for simulating the identical meteorological fields. E and L indicate Eulerian- and Lagrangian-based models, respectively. OD and ND indicate models that have their own dynamical (OD) core or have no dynamical core (ND), respectively. z, η, and σ indicate the height coordinate, η-coordinate, and σ-coordinate systems.

Model Name (E/L*1, OD/ND*2)	Resolution		Model top (Layer number)	Reference(s)
	Horizontal	Vertical*3		
AIST-MM(E, OD)	1 km	$\Delta z = 10 \sim 300$ m	5400 m (35)	Kondo et al. (2001)
ldX(E,ND)	1 km	$\Delta z = 40 \sim 600$ m	5000 m (17)	Mathieu et al. (2012)
GEARN(L,OD)	1 km	$\Delta\eta = 0.003 \sim 0.019/\Delta z = 20 \sim 678$ m*1	100 hPa (30)/15000 m (43)*1	Terada et al. (2020)
WRF-Chem-J (E,OD)	1 km	$\Delta\sigma = 0.0022 \sim 0.0073$	100 hPa (49)	Grell et al. (2005)
NHM-Chem(E, ND)	1 km	$\Delta\sigma = 0.002 \sim 0.03$	18000 m (55)	Kajino et al. (2019a, 2019b)
WRF-CMAQ(E, OD)	1 km	$\Delta\sigma = 0.007 \sim 0.013$	100 hPa (34)	Morino et al. (2013)
SCALE*2(E, OD)	1 km	$\Delta\sigma = 0.005 \sim 0.1$ $\Delta z = 40 \sim 656$ m*2	10000 m (19) 20184 m (58) *2	Kajino et al. (2019a, 2019b) Nishizawa et al. (2015) Sato et al. (2015)
WRF-Chem-T (E,OD)	1 km	$\Delta\sigma = 0.0026 \sim 0.0332$	100 hPa (30)	Hu et al. (2014)
NICAM(E,OD)	1 km	$\Delta z = 13.7 \sim 780$ m	22619 m (58)	Satoh et al. (2014) Uchida et al. (2017)
NHM-LETKF	1 km	$\Delta z = 40 \sim 656$ m	20200 m (58)	Sekiyama and Kajino (2020)

*1: GEARN used the η -coordinate system for its dynamical core and the height-coordinate system for its dispersion model. *2: SCALE was updated from the 2nd MIP to version 5.3.3; the meteorological field was calculated by its dynamical core with the z-coordinate system, and the radionuclide processes were calculated by offline coupling with NHM-Chem (Kajino et al., 2019a, 2019b), which uses the σ-coordinate system.

results of the atmospheric dispersion models (Wang et al., 2019). This is also true in simulated ^{137}Cs especially vertical diffusion of it, and the identical vertical resolution should be used to fully understand the reason of the uncertainties of the model. However, the vertical coordinate system was also different from model to model, and it is difficult to set an identical vertical resolution for all participated models. We should examine the uncertainty originated from the difference in the vertical grid resolution as a future study.

The meteorological field simulated by the operational weather forecast model of the Japan Meteorological Agency (JMA) and the non-hydrostatic model (NHM) coupled with an assimilation system based on the local ensemble Kalman filter (LETKF) (NHM-LETKF) with a grid spacing of 1 km (Sekiyama and Kajino, 2020) was used by all participating models. The meteorological field of NHM-LETKF was calculated by using the same assimilation system and the same data for the assimilation as those in the 2nd MIP whose grid spacing is 3 km (Sekiyama et al., 2017). Sekiyama and Kajino (2020) successfully increased reproducibility of the wind field by using the fine horizontal grid spacing and the fine topography. The detailed descriptions about the meteorological data are shown in Sekiyama and Kajino (2020).

The meteorological data were used to set the initial and boundary conditions, and nudging data for the models with their own dynamical core (OD models), or the data were used directly for dispersion models without their own dynamical core (ND models). The source term of ^{137}Cs (Katata et al., 2015) was used for all models, as in the 2nd MIP. All dispersion models except for GEARN were of the Eulerian type. GEARN is Lagrangian type dispersion model. In the 2nd MIP, we compared the performance of Eulerian type and that of Lagrangian type models and found no significant difference between the types. Such a comparison was not made because the number of Lagrangian type model was just one in the 3rd MIP. The calculation domain is shown in Fig. 1, with all models employing the same grid interval of 1 km (typically, 360 × 375 horizontal grid), although the vertical grid spacing was not common. The calculation period was from 00 UTC on 11 March 2011 to 00 UTC on 24 March 2011. The model results were output every hour.

In the 2nd MIP, Sato et al. (2018) evaluated the multimodel ensemble calculated by a weighting method and highlighted the advantage of using a score-weighted multimodel ensemble. Goto et al. (2020) evaluated the method used to calculate the multimodel ensemble. However, even if we selected the multimodel ensemble with equal weight, the performance of multimodel ensemble was better than most of the models in the 2nd MIP, and the multimodel ensemble with equal weight is sufficient to show the advantage of the multimodel ensemble. Thus, we used a multimodel ensemble with equal weights for all models because the main purpose of this study was to provide an overview of the 3rd MIP.

2.2. Selection of the source term

In this study, we used the source term of Katata et al. (2015) as in the 2nd MIP. Several previous studies proposed other source terms and discussed the uncertainties of the source term (e.g., Aoyama et al., 2016; Buesseler et al., 2017; Maki, 2015; Stohl et al., 2012; Terada et al., 2020). The source term estimated by each study differs from each other, and therefore, the source term is one of the largest factors of the uncertainties as well as the grid resolution and the meteorological field. Further efforts to improve the source term are required. However, our studies (the 2nd and the 3rd MIP) target on model's internal elements responsible for the uncertainties of the simulated ^{137}Cs (e.g., the physical process of ^{137}Cs such as dry deposition and wet deposition). Since the source term is one of the external elements, the selection of the source term is the out of scope of this study. Thus, we used same source term of Katata et al. (2015) as in the 2nd MIP study.

2.3. Observational data

To evaluate the models, this study used observational data for surface wind fields measured by the Automated Meteorological Data Acquisition System (AMeDAS) operated by the JMA, ^{137}Cs deposition obtained from aircraft measurements (MEXT, 2011), and atmospheric ^{137}Cs measurements made at 99 SPM sites (Oura et al., 2015). These data were also used in the 2nd MIP (Sato et al., 2018). In addition, observational data from two SPM measurement sites (Tsuruta et al., 2018) and wind fields measured at FDNPP by Tokyo Electric Power Company Holdings (TEPCO) were also used. Tsuruta et al. (2018) measured atmospheric ^{137}Cs concentrations at Futaba and Naraha, which are 3.2 km to the northwest and 17.5 km to the south of FDNPP, respectively. The Futaba site was too close to use in the evaluation of the model, so those data were not used. The location of the observational sites used by Oura et al. (2015), Tsuruta et al. (2018), and FDNPP are shown as black circles, black squares, and red crosses, respectively, in Fig. 1b. Hourly observational data were used. The AMeDAS wind field data were averaged over the previous hour based on values recorded every 10 min.

2.4. Evaluation

The performance of each model and the multimodel ensemble was evaluated using the same scores as those used by Sato et al. (2018) to show the advances made in the 3rd MIP compared to the 2nd MIP. The scores were named RANK and RANK2 for the cumulative deposition and atmospheric concentration of ^{137}Cs, respectively. The RANK and RANK2 scores were created by combining several scores to evaluate atmospheric

dispersion models (Sato et al., 2018). The definitions of RANK and RANK2 were as follows:

$$\mathrm{RANK} = \mathrm{CC}^2 + (1 - |\mathrm{FB}/2|) + \mathrm{FMS}/100 + (1 - \mathrm{KSP}/100), \quad (1)$$

$$\mathrm{RANK2} = \mathrm{FA2}/100 + \mathrm{CAPTURE}/100 + F \times (1\text{-}\mathrm{OVER}/100), \quad (2)$$

where CC, FB, FMS, KSP, FA2, CAPTURE, and OVER are correlation coefficient, fractional bias, figure of merit in space, Kolmogorov–Smirnov parameter, factor 2, capture rate, and overestimate rate, respectively. F is 0 when OVER is 0; otherwise F is 1. The detailed definition of each score is shown in supplementary material and Sato et al. (2018). In addition to the evaluation based on the ^{137}Cs concentrations, the wind field was evaluated using a Taylor diagram (Taylor, 2001).

In Section 3.1, the evaluations for the whole calculation period and the whole calculation domain are explained to enable an overview of the results of the models used in the 3rd MIP. Next, in Section 3.2, the performance of the models for the plumes observed near FDNPP (e.g., Hamadori; Fig. 1b) was evaluated, as no evaluation of these plumes was conducted by Sato et al. (2018). The newly evaluated plumes were plumes 1, 5, and 6 (P1, P5, and P6 as defined by Tsuruta et al., 2014). The performance of the models for other plumes was also evaluated and compared with that in the 2nd MIP. The recorded occurrences of P1, P5, and P6 were "12 March 08 Japan Standard Time (JST) to 13 March 05 JST," "18 March 04 JST to 18 March 23 JST," and "19 March 09 JST to 20 March 04 JST," respectively. The details of the plumes were described in Tsuruta et al. (2014). The target analysis area for the three plumes was "37.3°N~38.0°N, 140.5°E~141.0°E," which covers the Hamadori area. The target analysis areas for other plumes were the same as in the 2nd MIP (P2, P3, P4, P7, P8, and P9), as shown in Table 3 of Sato et al. (2018). Plume area was defined as the grid for which the surface atmospheric ^{137}Cs concentration exceeded 10 Bq m^{-3}, which is 10 times larger than that of the lower limit of the observation by SPM with confidence (Oura et al., 2015).

Because the grid points of the models were not always defined at the same point in the observation site, the model values subjected to the comparison were calculated as follows. First, we determined a model's grid point for which the latitude and longitude were nearest to those of the observation site. Next, the model concentration value being compared was calculated as the average of 3 × 3 grids with the nearest grid at the center, as in Sato et al. (2018).

3. Results

3.1. Evaluation of the whole calculation domain during the whole calculation period

We evaluated the averaged model performance during the whole calculation period and over the whole calculation domain to provide an overview of the results of the 3rd MIP. Fig. 2 shows the cumulative deposition of ^{137}Cs observed by aircraft measurement (Fig. 2a) and that simulated by the multimodel ensemble accumulated from 00 UTC on 11 March to 00 UTC on 24 March (Fig. 2b). The results of each model are shown in the appendix (Fig. S1). The results of the multimodel ensemble used in the 2nd MIP accumulated from 11 March to 00 UTC on 24 March are also shown in Fig. 2c. The observed cumulative deposition was measured from June to November 2011, which was different from the calculation period. However, the deposition of ^{137}Cs in March after the calculation period (i.e., from 00 UTC on 11 March to 00 UTC on 24 March 2011) was low based on the analyses of the 2nd MIP (Sato et al., 2018), and deposition in April to June was also low (Morino et al., 2013). Thus, the comparison between the aircraft measurements and the simulated results was acceptable.

Compared with the results of the 2nd MIP, the models simulated the narrow distribution of high deposition (i.e., exceeding 10^5 Bq m^{-2}) to the northwest of FDNPP reasonably well. In addition, the overestimation over the area to the south of FDNPP was considerably reduced. These two improvements probably originated from the use of a finer grid resolution in the 3rd MIP. The large horizontal diffusion obtained using the coarse grid resolution in the previous study resulted in a broader distribution of atmospheric ^{137}Cs and hence a wider distribution of deposition. This was one of the improvements over the 2nd MIP made in this study. Despite these improvements, the overestimation over the northern part of the Tokyo Metropolitan Area (TMA) and the underestimations over the Nakadori area and the northern part of Gunma and Tochigi Prefectures were either not improved or were even worse than in the 2nd MIP. These results imply that the finer grid resolution in both the meteorological and dispersion simulations did not necessarily improve deposition patterns over areas more than several tens of kilometers from the source, although the finer representation of topography significantly improved the representation of the plume around FDNPP, as we discuss later.

The RANK score of the multimodel ensemble was 2.72, which was worse than that in the 2nd MIP (3.21), and most of the models had the same trend (Appendix, Table S1). From these results, we can conclude that the performance of the models in the 3rd MIP was poor relative to that of the models in the 2nd MIP with respect to the cumulative deposition in the whole calculation domain. This reduced performance mainly originated from the poor representation of deposition over the

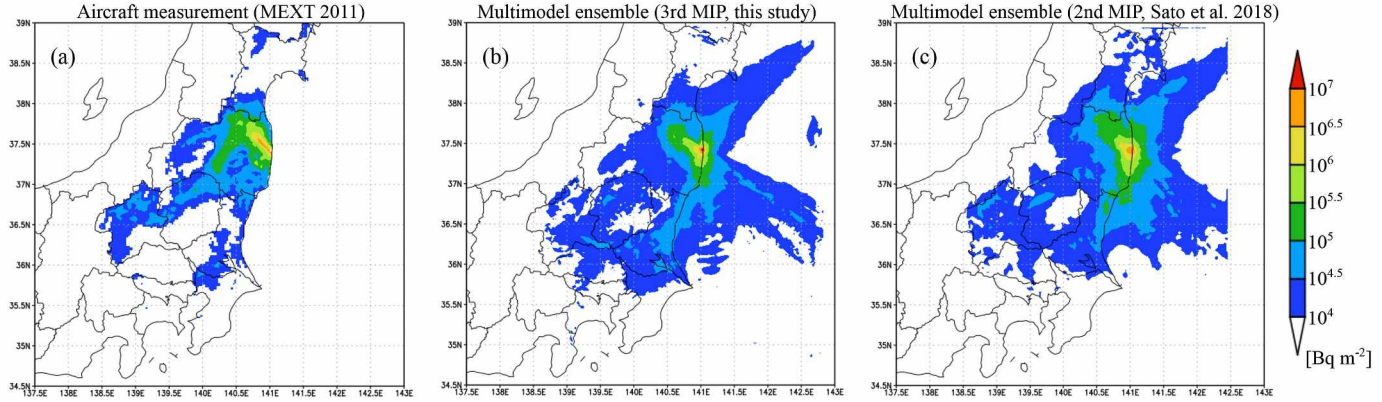

Fig. 2. Geographical distribution of the cumulative deposition of ^{137}Cs (a) observed by aircraft measurement, (b) created from the results of the multimodel ensemble in this study, and (c) created from the results of the multimodel ensemble in the 2nd MIP (Sato et al., 2018). The maps in the figures were constructed using the Grid Analysis and Display System (GrADS: Institute for Global Environment and Society (IGES), 1989).

area far from FDNPP i.e. TMA.

Although the performance in terms of the cumulative deposition in the 3rd MIP was worse, models that perform well for cumulative deposition do not always perform well in terms of atmospheric concentration, and vice versa (Draxler et al., 2015). Therefore, we next evaluated the performance of the models in terms of atmospheric concentrations. Fig. 3a shows a composite of the temporal evolution of the atmospheric ^{137}Cs concentrations normalized by the observed values at 99 SPM sites (Oura et al., 2015) during the whole period of the simulation. The temporal evolution of the plumes was well simulated, and the timing of the plume arrival simulated by the models was a few hours later than the observation in the 3rd MIP as in the 2nd MIP. The timing and concentrations at Naraha station were successfully simulated (Fig. 3b). The delay of the plume arrival at most of the stations was seen in both Fukushima area and TMA. As well as the time delay, we should note that the simulated ^{137}Cs maintained high concentration level after the plume arrival, although observed ^{137}Cs reduced after the plume arrival. These trends were similar to the results of the 2nd MIP, and therefore, we speculate that these trends were originated from the uncertainties in source term. Thus, the further improvement of the source term is required. In spite of the delay of the plume arrival, we can conclude that the models in the 3rd MIP successfully simulated the plume arrival for SPM sites as in the 2nd MIP.

3.2. Evaluation for plumes near FDNPP

The successful simulation of the temporal evolution of atmospheric ^{137}Cs concentrations encouraged us to evaluate the models' performance for each plume. In this study, we first focused on the plumes observed near FDNPP, i.e., P1, P5, and P6. The evaluation of these plumes was itself one of the advances from the 2nd MIP.

No precipitation was observed during the period when these plumes passed over the Hamadori area, where they were observed. Therefore, any contribution of wet deposition to a reduction in the atmospheric ^{137}Cs concentrations during the passage of the plumes can be ignored. The RANK2 scores of the multimodel ensemble were 1.42, 1.10, and 1.76 for P1, P5, and P6, respectively (Table 2). A breakdown of the RANK2 scores is provided in the Appendix (Table S2). It should be noted that although the RANK2 scores of the multimodel ensemble for all these plumes exceeded 1.00, the RANK2 score of some models was 0.0 because these models completely missed the plume. This tendency was clearest in P6. For P6, four models completely missed the plume, but its RANK2 score in the multimodel ensemble was the highest of the three plumes. The high RANK2 score of the multimodel ensemble was achieved by the reasonable simulation of the ^{137}Cs concentrations by some other models. These results indicate that error of most of the models was cancelled out through averaging, and the results imply that the multimodel ensemble had an advantage over the individual models in simulating plumes.

Table 2
RANK2 scores for Plume 1, Plume 5, and Plume 6.

Model	Plume 1	Plume 5	Plume 6
AIST-MM	0.57	0.41	1.12
IdX	0.51	0.13	1.17
GEARN	0.91	1.38	0.48
WRF-Chem-J	0.31	0.74	0.69
NHM-Chem	0.0	0.31	0.0
WRF-CMAQ	0.0	0.0	0.0
SCALE	1.79	0.0	1.77
WRF-Chem-T	0.94	0.12	0.0
NICAM	0.41	0.13	0.0
Ensemble Mean	1.42	1.10	1.76

To understand the reason for the differences in performance among the models, the geographical distribution of atmospheric ^{137}Cs concentrations simulated by each model is useful. Fig. 4 shows the geographical distribution of atmospheric ^{137}Cs concentrations and the wind field at 11 JST on 19 March 2011 (P6), obtained from the multimodel ensemble. The SCALE and NHM-Chem results are also shown in Fig. 4 and are representative of models with high and low RANK2 scores, respectively. In the SCALE results, a line of discontinuity in wind direction, which corresponds to a local frontal structure, was simulated over the western part of the Hamadori area, i.e., the eastern edge of the Abukuma Plateau (Fig. 5c). An area with high ^{137}Cs concentrations was simulated to the east of the line, including the SPM sites in the Hamadori area, where high concentrations were observed. In contrast, in the NHM-Chem results, the line of the wind direction discontinuity was simulated as being over the coastline, i.e., the local front was simulated more to the east by NHM-Chem than by SCALE. The ^{137}Cs was sourced from the eastern side of the local front, and the discharged ^{137}Cs could not be

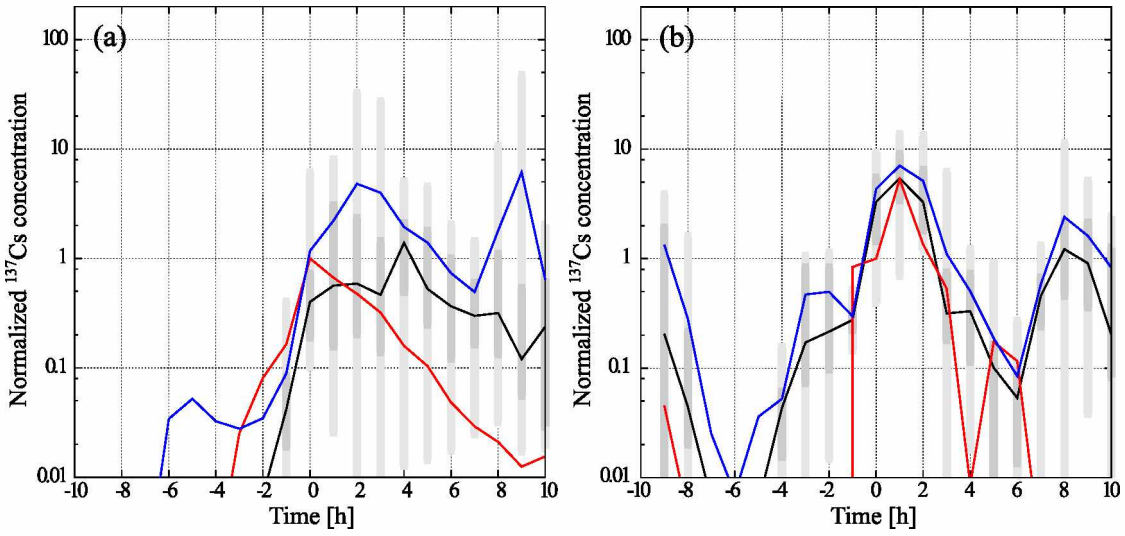

Fig. 3. Temporal evolution of atmospheric ^{137}Cs concentrations, normalized by the observed values averaged during the entire calculation time and averaged over (a) the SPM site used by Oura et al. (2015) in the calculation domain and (b) the Naraha SPM sites used by Tsuruta et al. (2018). Time (t) = 0 is the time point when a high ^{137}Cs concentration event (>100 Bq m^{-3}) was observed. The red, blue, and black lines show the observed values, model ensemble means, and medians of the models, respectively. The thick and thin grey bars indicate the range of the 25th to 75th percentiles and the minimum to maximum, respectively. (For interpretation of the references to colour in this figure legend, the reader is referred to the Web version of this article.)

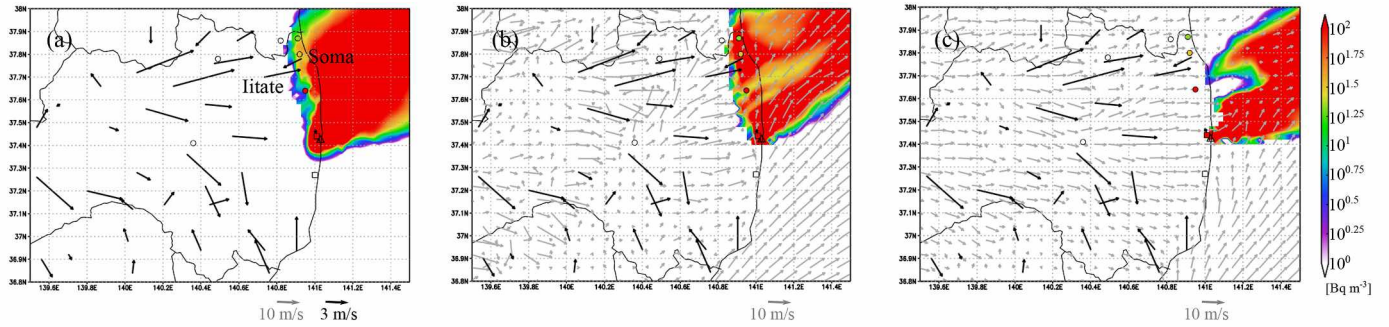

Fig. 4. (Shade) Geographical distribution of ^{137}Cs and (grey arrow) the wind field at a height of 10 m at 11 JST on 19 March 2011 simulated by (a) the multimodel ensemble, (b) SCALE, and (c) NHM-Chem. The circles and squares show the atmospheric ^{137}Cs concentrations measured at the SPM sites used by Oura et al. (2015) and Tsuruta et al. (2018), respectively. The open triangle and black arrows in (a) show the locations of FDNPP and the surface wind field observed by AMeDAS and TEPCO, respectively. The arrows below each figure show the scale of wind velocity. The maps in the figures were constructed using the Grid Analysis and Display System (GrADS: Institute for Global Environment and Society (IGES), 1989). (For interpretation of the references to colour in this figure legend, the reader is referred to the Web version of this article.)

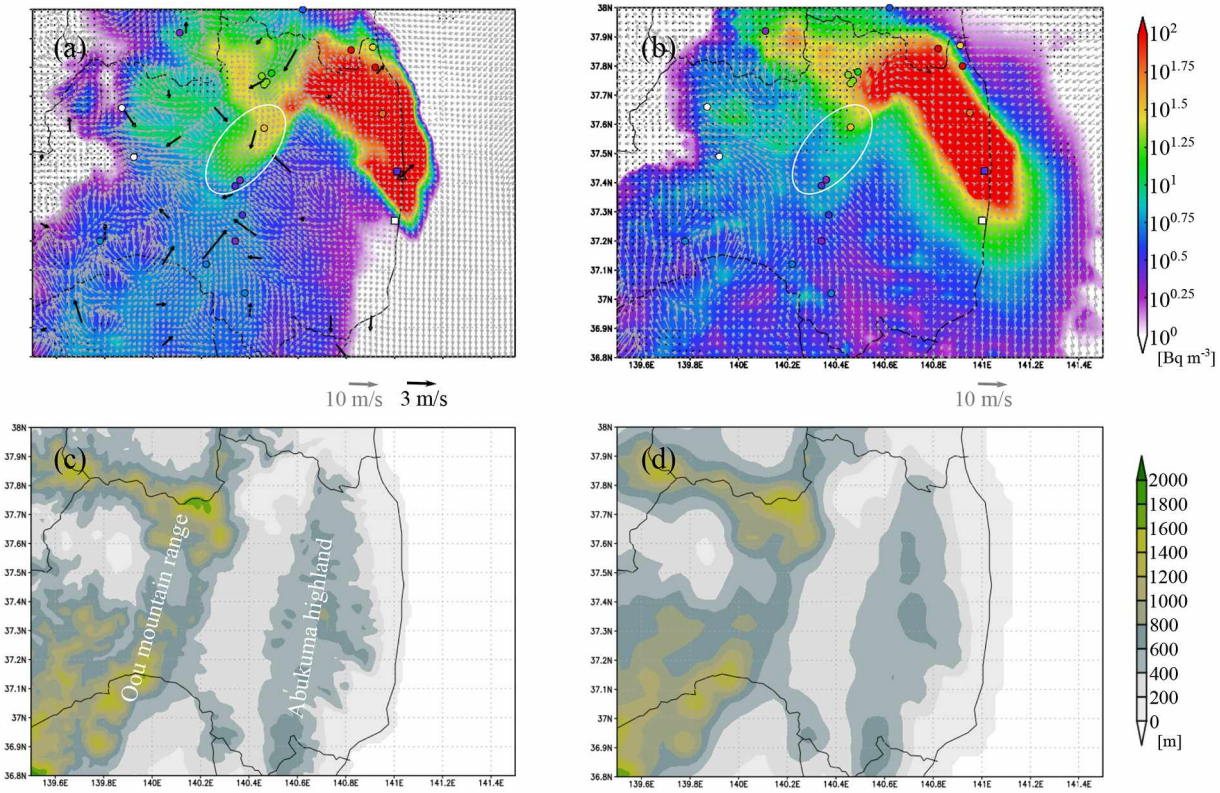

Fig. 5. (a, b) (Shade) Geographical distribution of ^{137}Cs and (grey arrow) the wind field at a height of 10 m at 19 JST on 20 March 2011 simulated by (a) the multimodel ensemble used in this study, and (b) the multimodel ensemble used in the 2nd MIP (Sato et al., 2018), and the elevation of the orography used by NHM-LETKF in (c) this study and (d) in the 2nd MIP (Sato et al., 2018). The circles and squares in (a) and (b) show the atmospheric ^{137}Cs concentrations measured at the SPM sites used by Oura et al. (2015) and Tsuruta et al. (2018), respectively. The open triangle and black arrows in (a) show the location of FDNPP and surface wind field observed by AMeDAS and TEPCO, respectively. The arrows below (a) and (b) show the scale of wind velocity. The white circles in (a) and (b) show the area discussed in the body of the manuscript. The maps in the figures were constructed using the Grid Analysis and Display System (GrADS: Institute for Global Environment and Society (IGES), 1989). (For interpretation of the references to colour in this figure legend, the reader is referred to the Web version of this article.)

transported across the front; hence, the plume did not reach the Hamadori area in the NHM-Chem simulation.

The AMeDAS data over the Hamadori area were not available due to the power failure that resulted from the earthquake. However, the AMeDAS observation data at the Soma and Iitate sites indicate that the wind directions at the two sites were opposite each other. This is evidence of the existence of a local frontal structure, which was seen in the SCALE simulation results over the eastern edge of the Abukuma Plateau. The location of the frontal system differed, even though all models used identical meteorological data. These differences originated from differences in the nudging method, vertical resolution, and other factors. These results indicate that the models that performed well reasonably reproduced the wind field, i.e., the location of the frontal line over the Hamadori area.

Of all the models, only SCALE clearly reproduced the location of the local frontal structure. Consequently, the RANK2 score of SCALE was better than those of the other models. The RANK2 scores of the models were mostly <1.00 for P6; however, the RANK2 score of the ensemble

mean was good (RANK2 = 1.76) due to the performance of SCALE (RANK2 = 1.77) and the other acceptable models (RANK2 = 1.12 to 1.17). This means that the improvement in the RANK2 score of the multimodel ensemble was mostly due to the good performance of SCALE. This improvement is a good example of the advantages of using a multimodel ensemble.

Differences in the position of the frontal line between the models with high and low RANK2 scores were also apparent during the P1 event (Fig. S3). It was difficult to validate our simulation results because meteorological data were not obtained due to the power failure, and no AMeDAS data were available for the Hamadori area, including the Soma and Iitate sites, during the P1 period. In general, the location of frontal lines strongly affects atmospheric dispersion fields. Based on the good RANK2 scores, it is considered likely that atmospheric ^{137}Cs transport in the P1 event was simulated reasonably well, as indicated by the acceptable wind field simulated by the better-performing models. Similarly, reasonable simulation of the wind field was also important for P5, as discussed in the supporting information (S1 and Fig. S3).

Based on the results reported in this section, we conclude that the wind field, including the location of the local front around the edge of the plateau, must be reproduced for reasonable simulation of P1, P5, and P6, which were measured near FDNPP. This conclusion of the 3rd MIP implies that representation of a local front is critical in simulating the atmospheric transport of radionuclides emitted from a nuclear facility located on the coast in the vicinity of highlands or mountainous areas. In Japan, these geographical features are common in areas near nuclear power plants.

3.3. *Evaluation of the plumes observed in the Nakadori area*

We evaluated the models' performance for the plumes observed over the Nakadori area (Fig. 1b), which is farther from FDNPP than is Hamadori, to show the differences between the 3rd MIP and the 2nd MIP. The plumes observed in this area were P3 and P8.

The RANK2 scores for the 2nd and 3rd MIPs are tabulated in Table 3. For P8, the RANK2 scores of about half of the models were higher in the 3rd MIP than in the 2nd MIP, while the other half of the models had lower scores in the 3rd MIP than in the 2nd MIP. Despite these results, the RANK2 score of the model for P8 in the 3rd MIP was 1.87, which was better than that in the 2nd MIP (1.57), as shown in Table 3. This result also shows the advantage of the multimodel ensemble. As we discussed with respect to the 2nd MIP (Sato et al., 2018), the ^{137}Cs in P8 was emitted from FDNPP around mid-day on 20 March (11:25 on 20 March; Katata et al., 2015). The emitted ^{137}Cs was first transported northwestward by a southeast wind. After being transported northwestward to Nakadori, the ^{137}Cs plume was advected to the southwest by a northeast wind, causing the high ^{137}Cs concentration measured over the Nakadori area. The geographical distribution of ^{137}Cs and the wind field near the surface simulated by the multimodel ensemble are shown in Fig. 5. The northeast wind through the Nakadori area is shown as the area enclosed within the white circle; the ^{137}Cs migration to the southwest due to the northeast wind was clearly reproduced by the 3rd MIP model ensemble (Fig. 5a). On the other hand, in the multimodel ensemble of the 2nd MIP, the northeast wind was not apparent, and the ^{137}Cs stagnated around the northern part of Fukushima Prefecture (Fig. 5b). These results indicate that the wind field was simulated more reasonably in the 3rd MIP than in the 2nd MIP. Additionally, Taylor (2001) produced a diagram that, with respect to the wind field, indicated that most models and the multimodel ensemble in the 3rd MIP had a smaller bias than did the 2nd MIP (Fig. 6). This comparison, based on the diagram, revealed a better reproduction of the wind field in the 3rd MIP than that in the 2nd MIP, implying that the atmospheric dispersion

Table 3
RANK2 scores for Plume 2, Plume 3, Plume 7, Plume 8, and Plume 9. The RANK2 scores of the 2nd MIP (Sato et al., 2018) are also shown. "-" means that the model did not participate in the 3rd MIP. The red and blue characters mean that the performance of the model in the 3rd MIP was better and worse than the 2nd MIP respectively.

	P2		P3		P4		P7		P8		P9	
Model	2nd	3rd	2nd	3rd	2nd	3rd	2nd	3rd	2nd	3rd	2nd	3rd
AIST-MM	0.93	1.25	0.12	0.00	1.07	0.39	1.08	0.00	0.81	1.13	0.00	1.01
PELLO	1.16	-	0.64	-	1.40	-	0.76	-	1.25	-	0.15	-
HIRAT	1.50	-	0.48	-	0.00	-	0.70	-	1.43	-	0.00	-
IdX	1.21	0.01	0.09	0.00	0.52	0.00	0.01	0.40	1.51	1.38	0.00	0.10
GEARN	1.31	1.40	0.34	0.00	1.31	0.00	0.79	0.79	1.71	1.56	0.35	0.18
WRF-Chem-J	1.45	0.89	0.58	0.16	0.00	0.50	0.90	0.81	1.42	1.67	0.00	0.06
NHM-Chem	0.92	1.28	0.37	0.18	1.72	0.00	0.45	0.08	1.64	2.00	0.00	0.14
WRF-CMAQ	1.12	1.54	1.15	0.00	0.00	0.00	1.04	0.67	1.88	1.12	0.00	0.76
SCALE	1.06	1.17	0.50	0.26	0.00	0.00	0.00	0.00	1.18	0.45	0.00	0.00
Polyphemus	0.72	-	1.35	-	0.00	-	0.00	-	1.18	-	0.00	-
WRF-Chem-T	1.52	1.28	0.25	0.03	0.00	0.00	0.00	0.67	2.15	2.01	1.37	1.12
NICAM	0.93	1.28	0.58	0.13	0.00	0.00	0.79	0.48	1.02	1.41	0.05	0.08
Ensemble Mean	1.61	1.36	1.07	0.00	1.24	0.76	0.78	0.55	1.57	1.87	0.14	0.29

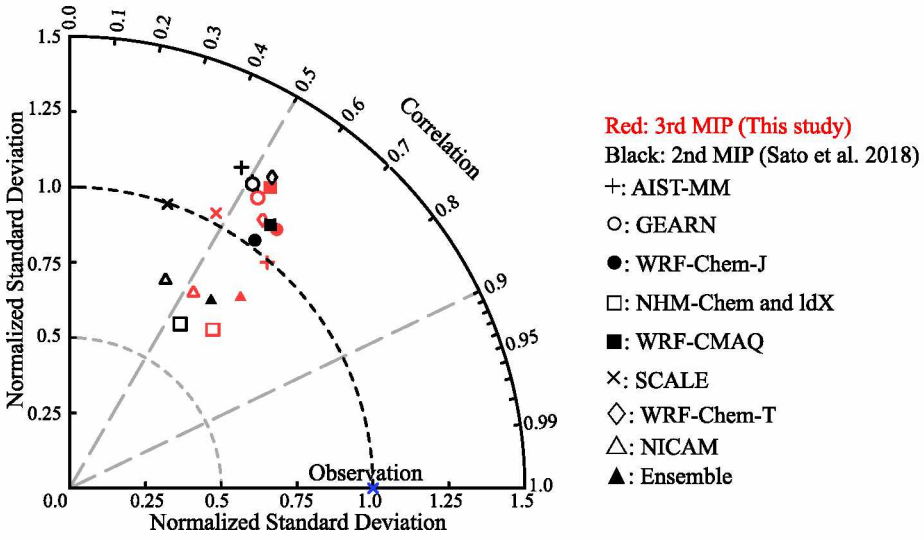

Fig. 6. Taylor diagram (Taylor, 2001) for the wind field of (plus) AIST-MM, (open circle) GEARN, (closed circle) WRF-Chem-J, (open square) NHM-Chem, (closed square), WRF-CMAQ, (cross) SCALE, (diamond) WRF-Chem-T, (open triangle) NICAM, and (closed triangle) the multimodel ensemble, during the plume 8 period in the Hamadori and Nakadori areas. Black and red symbols indicate the results of the 2nd MIP (Sato et al., 2018) and the 3rd MIP, respectively. Blue cross indicates the observed result. To create the diagram, all available AMeDAS data over the target area and during the P8 target period were used. (For interpretation of the references to colour in this figure legend, the reader is referred to the Web version of this article.)

of ^{137}Cs was more reasonable in the present study than in the previous one. Some models performed worse in the 3rd MIP. For example, the relatively poor performance of WRF-Chem-J originated from the nudging method. In the 2nd MIP, WRF-Chem-J used AMeDAS data for nudging as well as the meteorological field of NHM-LETKF. On the other hand, AMeDAS data were not used in the 3rd MIP. However, the performance of most models with respect to the wind field was improved from the 2nd MIP. From these results, it was concluded that the lower RANK2 score of the 2nd MIP originated from the poor representation of the northeast wind passing through the Nakadori area. Improvement of the wind field using a fine grid resolution contributed to the improved performance of the models in the 3rd MIP. The reasonable simulation of the wind field in the 3rd MIP originated from better expression of the topography, as discussed in Sekiyama and Kajino (2020). The Nakadori area corresponds to the Fukushima and Koriyama basins, which are located between the Abukuma Plateau to the east and the Oou mountain range to the west, and the northeast wind was a valley breeze passing through the Nakadori area. Expression of the mountain using a fine grid resolution (Fig. 5c) allowed the valley breeze to be better simulated than was possible using a coarse grid resolution (Fig. 5d).

In addition, we revisited the issues discussed in our previous study (Sato et al., 2018), where we indicated that a lower deposition rate during transport from FDNPP to the Nakadori area is required to reproduce P8. We now consider that this remark should be modified. In the 2nd MIP, the northeast wind was not clearly reproduced, as discussed above, and atmospheric ^{137}Cs tended to stagnate around the northern part of the Nakadori area. Due to this stagnation, the ^{137}Cs concentration in the northern part of Fukushima Prefecture was small in the 2nd MIP. In this case, the presumed stagnation led to depletion of ^{137}Cs through deposition in the northern part of Fukushima Prefecture. In contrast, in the 3rd MIP, the northeast wind, which was captured by the AMeDAS surface wind observation depicted in Fig. 5a, was well reproduced, and ^{137}Cs was advected to the Nakadori area with little deposition. Thus, low deposition is not a necessary condition for the reasonable simulation of P8.

In contrast to the model performance for P8, the performance for P3 was much worse in this study than in the 2nd MIP (Table 3). As we discussed in the 2nd MIP report (see the Supporting Information S2.1 of Sato et al. (2018)), the ^{137}Cs in P3 was transported to the Nakadori area as follows. The ^{137}Cs emitted from FDNPP on the morning of 15 March (from 06 JST to 12 JST on 15 March, Katata et al., 2015) was first transported southwest by a northeast wind. Around noon on 15 March, the wind direction changed to a southeast wind. The southeast wind transported the ^{137}Cs to the Nakadori area, and P3 reached the Nakadori area. Sato et al. (2018) reported that the model performance was not good for P3 due to a delay in the change in the wind direction in the 2nd MIP. Such a delay was also seen in the 3rd MIP (figure not shown) and was very significant in terms of the poor performance of the model. Although the delay was seen in both the 2nd and 3rd MIPs, the score was much worse in the 3rd MIP.

The geographical distributions of atmospheric ^{137}Cs and the wind field shown in Fig. 7 also help to explain the poorer performance in the 3rd MIP. As can be seen from Fig. 7, the differences in the wind field and plume location between the results of the 2nd and those of the 3rd MIPs were small, but the area with a large ^{137}Cs concentration (i.e., exceeding 10 Bq m^{-3}) was smaller in the 3rd MIP than in the 2nd MIP. The difference in the ^{137}Cs distribution originated from differences in horizontal diffusion. As discussed in Section 3.1., a coarse horizontal grid spacing typically generates large horizontal diffusion, resulting in a wide distribution of a tracer. The smaller horizontal diffusion in the 3rd MIP resulted in a narrower plume area. In contrast, the greater diffusion in the 2nd MIP due to the coarse horizontal grid resolution resulted in a wider plume area. In addition to the large diffusion that originated due to the coarse grid resolution, some models with large diffusion (i.e., Polyphemus and HIRAT-LPRM, see Table 1 of Sato et al., 2018 for the details of the models) were included in the 2nd MIP model ensemble. The area with high ^{137}Cs concentration as simulated by these models was significantly wider than that simulated by the other models. Such models also contributed to the wider area with a large ^{137}Cs in the 2nd MIP. Due to the wider area with a large ^{137}Cs concentration in the 2nd MIP, the northern edge of the plume area in the 2nd MIP reached the Nakadori area (Fig. 7b), so the performance was considered better in the 2nd MIP than in the 3rd MIP. A better score for models with large diffusion was also reported by the European Tracer Experiment (ETEX: Graziani et al., 1998), and it is therefore important to pay attention to the impact of horizontal diffusion on statistical scores.

3.4. Plume observed over the Tokyo Metropolitan Area (TMA)

We evaluated the models' performance for the plumes observed over the TMA (i.e., P2, P4, P7, and P9), where the distance from FDNPP is much greater than that of the Nakadori and Hamadori areas. For P2, two-thirds of the models improved their performance based on the RANK2 scores (Table 3) when using meteorological data with a fine grid resolution. Despite the improvement in some models for P2, the RANK2 scores of all models were worse for P4, and most of the models (except

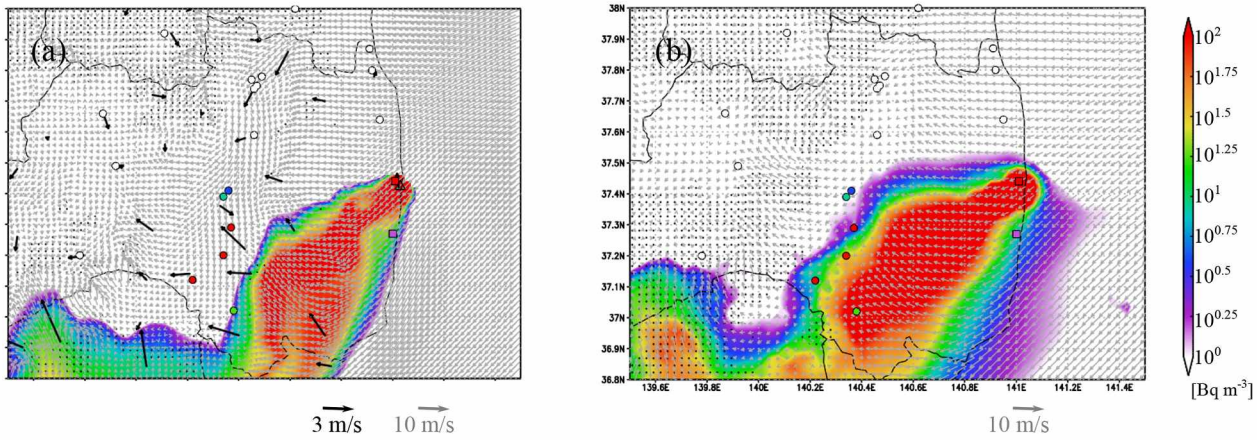

Fig. 7. Same as Fig. 5a and 5b but for 14 JST on 15 March 2011.

two) performed poorly for P7. The RANK2 scores for P9 in both the 2nd and 3rd MIPs were low, and the improvement in P9 from the 2nd to the 3rd MIP was considered insignificant. Due to the poorer scores of each model, the RANK2 scores of the multimodel ensemble for the plumes observed over the TMA were lower in the 3rd MIP than in the 2nd MIP (Table 3). As discussed by Sekiyama and Kajino (2020), the drop in performance was because of the poorer representation of the wind field over TMA in the meteorological data with a 1-km grid resolution than would be possible with a 3-km grid resolution. The overall reason for the worse performance was not clarified other than to note that a few of the models with better performance in the 2nd MIP were absent from the 3rd MIP ensemble. A further investigation of the reason for the poor representation of the wind field and poorer model performance for the plumes will be the focus of a future study.

As well as the investigation of the poor performance of the model, the improvement of the meteorological fields is also important for reasonable simulation of the plumes. The advance in the data assimilation is also required for calculating the better meteorological field. This is also a topic of our future study.

However, we can provide several suggestions for future modelers based on the analyses conducted in this study.

- In the vicinity of FDNPP, meteorological field and atmospheric dispersion calculations with a fine (1 km or less) grid resolution are needed to evaluate and investigate the atmospheric behavior of atmospheric ^{137}Cs.
- The use of meteorological data with a fine grid resolution does not always improve the performance of a model compared to the use of a coarser resolution, especially for areas distant from the source.

4. Conclusion

In this study, a new model intercomparison targeting the atmospheric ^{137}Cs emitted from FDNPP in March 2011 (3rd MIP) was conducted using the same meteorological field (Sekiyama and Kajino, 2020) and emission inventory (Katata et al., 2015). Nine models that were included in the 2nd MIP were also used in the 3rd MIP. One advance in the 3rd MIP compared to the 2nd MIP was the use of a finer horizontal grid spacing (2 km finer than that of the 2nd MIP (3 km). The finer grid spacing enabled us to evaluate the models' performance for the plumes observed near FDNPP, i.e., the Hamadori area. In addition, we used data for the Futaba and Naraha SPM sites (Tsuruta et al., 2018), which are near FDNPP, for the evaluation of the models.

The analyses indicated that the participating models simulated the temporal evolution of atmospheric ^{137}Cs concentration measured at SPM sites well, with a few hours delay, as was also observed in the results of the 2nd MIP. The evaluation of the models' performance for the P1, P5, and P6 plumes observed over the Hamadori area (Tsuruta et al., 2014) was first conducted through a comparison of the results of the models with observational data. The analyses indicated that the model with the best performance (SCALE) simulated a local front observed as a discontinuity line in the wind direction over the Hamadori area reasonably well. Due to this better simulation of the wind field by SCALE, the ^{137}Cs plume transported from FDNPP to the Hamadori area was reasonably well represented by the multimodel ensemble in the 3rd MIP.

Our analyses also confirmed that the models in the 3rd MIP simulated P8, which was observed over the Nakadori area (Tsuruta et al., 2014), more successfully than did those in the 2nd MIP. The improved performance originated from an increase in the reproducibility of the northeast wind that passed through the Nakadori area, which was probably due to the high-resolution terrain in the models. The overall performance of the multimodel ensemble was better than the individual performance of each model.

Our analyses also indicated that the models' performance in terms of the cumulative deposition and the atmospheric concentration of plumes observed at sites far from FDNPP (TMA) was worse than those of the 2nd MIP. This indicates that a finer grid resolution does not always improve the performance of a model, although a simulation with a finer grid resolution was necessary to accurately simulate the plumes observed near FDNPP and evaluate the models used to simulate the plumes.

Data availability

All data used in this study are stored on servers of Hokkaido University, Nagoya University, and JAMSTEC, and the data can be used for scientific purposes upon reasonable request to Yousuke Sato and Hiromi Yamazawa.

CRediT authorship contribution statement

Yousuke Sato: Conceptualization, Data curation, Formal analysis, Methodology, Resources, Software, Validation, Visualization, Writing - original draft. **Tsuyoshi Thomas Sekiyama:** Methodology, Resources, Software, Validation. **Sheng Fang:** Methodology, Resources, Software, Validation. **Mizuo Kajino:** Methodology, Resources, Software, Validation. **Arnaud Quérel:** Methodology, Resources, Software, Validation. **Denis Quélo:** Methodology, Resources, Software, Supervision. **Hiroaki Kondo:** Methodology, Resources, Software, Validation. **Hiroaki Terada:** Methodology, Resources, Software, Validation. **Masanao Kadowaki:** Methodology, Resources, Software, Validation. **Masayuki Takigawa:** Methodology, Resources, Software, Validation. **Yu Morino:** Methodology, Resources, Software, Validation. **Junya Uchida:** Methodology, Resources, Software, Validation. **Daisuke Goto:** Methodology,

Resources, Software, Validation. **Hiromi Yamazawa:** Conceptualization, Funding acquisition, Project administration, Supervision, Writing - review & editing.

Declaration of competing interest

The authors declare that they have no known competing financial interests or personal relationships that could have appeared to influence the work reported in this paper.

Acknowledgement

This research is supported by Environment Research and Technology Development Fund (Grant number : JPMEERF20155001, JPMEERF20181002) of the Environmental Restoration and Conservation Agency of Japan and JSPS KAKENHI (Grant Number 17K00533, 18K11633, 19H01155). Yousuke Sato is supported by the fund of Research Field of Hokkaido Weather Forecast and Technology Development (endowed by Hokkaido Weather Technology Center Co. Ltd.). The data of wind field at FDNPP is downloadable from website of TEPCO Holdings (http://www.tepco.co.jp/cc/press/betu11_j/images/110528d.pdf, accessed on April 3, 2020). Sheng Fang is supported by the National Natural Science Foundations of China (Grant Number 11875037) and IAEA TC project CRP9053. The computational resources were provided for some of the authors from the National Institute for Environmental Studies.

Appendix A. Supplementary data

Supplementary data to this article can be found online at https://doi.org/10.1016/j.aeaoa.2020.100086.

References

Ackerman, A.S., VanZanten, M.C., Stevens, B., Savic-Jovcic, V., Bretherton, C.S., Chlond, A., Golaz, J.-C., Jiang, H., Khairoutdinov, M., Krueger, S.K., Lewellen, D.C., Lock, A., Moeng, C.-H., Nakamura, K., Petters, M.D., Snider, J.R., Weinbrecht, S., Zulauf, M., 2009. Large-eddy simulations of a drizzling, stratocumulus-topped marine boundary layer. Mon. Weather Rev. 137, 1083–1110. https://doi.org/10.1175/2008MWR2582.1.

Adachi, K., Kajino, M., Zaizen, Y., Igarashi, Y., 2013. Emission of spherical cesium-bearing particles from an early stage of the Fukushima nuclear accident. Sci. Rep. 3, 2554. https://doi.org/10.1038/srep02554.

Aoyama, M., Hamajima, Y., Hult, M., Uematsu, M., Oka, E., Tsumune, D., Kumamoto, Y., 2016. 134Cs and 137Cs in the north pacific ocean derived from the March 2011 TEPCO Fukushima Dai-ichi nuclear power plant accident, Japan. Part one: surface pathway and vertical distributions. J. Oceanogr. 72, 53–65. https://doi.org/10.1007/s10872-015-0335-z.

Arnold, D., Maurer, C., Wotawa, G., Draxler, R., Saito, K., Seibert, P., 2015. Influence of the meteorological input on the atmospheric transport modelling with FLEXPART of radionuclides from the Fukushima Daiichi nuclear accident. J. Environ. Radioact. 139, 212–225. https://doi.org/10.1016/j.jenvrad.2014.02.013.

Bessagnet, B., Pirovano, G., Mircea, M., Cuvelier, C., Aulinger, A., Calori, G., Ciarelli, G., Manders, A., Stern, R., Tsyro, S., García Vivanco, M., Thunis, P., Pay, M.-T., Colette, A., Couvidat, F., Meleux, F., Rouïl, L., Ung, A., Aksoyoglu, S., Baldasano, J. M., Bieser, J., Briganti, G., Cappelletti, A., D'Isidoro, M., Finardi, S., Kranenburg, R., Silibello, C., Carnevale, C., Aas, W., Dupont, J.-C., Fagerli, H., Gonzalez, L., Menut, L., Prévôt, A.S.H., Roberts, P., White, L., 2016. Presentation of the EURODELTA III intercomparison exercise – evaluation of the chemistry transport models' performance on criteria pollutants and joint analysis with meteorology. Atmos. Chem. Phys. 16, 12667–12701. https://doi.org/10.5194/acp-16-12667-2016.

Blossey, P.N., Bretherton, C.S., Zhang, M., Cheng, A., Endo, S., Heus, T., Liu, Y., Lock, A. P., De Roode, S.R., Xu, K.M., 2013. Marine low cloud sensitivity to an idealized climate change: the CGILS les intercomparison. J. Adv. Model. Earth Syst. 5, 234–258. https://doi.org/10.1002/jame.20025.

Bretherton, C.S., Krueger, S.K., Wyant, M.C., Bechtold, P., Van Meijgaard, E., Stevens, B., Teixeira, J., 1999. A GCSS boundary-layer cloud model intercomparison study of the first ASTEX Lagrangian experiment. Boundary-Layer Meteorol. 93, 341–380.

Buesseler, K., Dai, M., Aoyama, M., Benitez-Nelson, C., Charmasson, S., Higley, K., Maderich, V., Masqué, P., Morris, P.J., Oughton, D., Smith, J.N., 2017. Fukushima Daiichi–Derived Radionuclides in the ocean: transport, fate, and impacts. Ann. Rev. Mar. Sci. 9, 173–203. https://doi.org/10.1146/annurev-marine-010816-060733.

Chino, M., Nakayama, H., Nagai, H., Terada, H., Katata, G., Yamazawa, H., 2011. Preliminary estimation of release amounts of 131 I and 137 Cs accidentally discharged from the Fukushima Daiichi Nuclear Power Plant into the atmosphere. J. Nucl. Sci. Technol. 48, 1129–1134. https://doi.org/10.1080/18811248.2011.9711799.

Dacre, H.F., Bedwell, P., Hertwig, D., Leadbetter, S.J., Loizou, P., Webster, H.N., 2020. Improved representation of particle size and solubility in model simulations of atmospheric dispersion and wet-deposition from Fukushima. J. Environ. Radioact. 217, 106193. https://doi.org/10.1016/j.jenvrad.2020.106193.

Dore, A.J., Carslaw, D.C., Braban, C., Cain, M., Chemel, C., Conolly, C., Derwent, R.G., Griffiths, S.J., Hall, J., Hayman, G., Lawrence, S., Metcalfe, S.E., Redington, A., Simpson, D., Sutton, M.A., Sutton, P., Tang, Y.S., Vieno, M., Werner, M., Whyatt, J. D., 2015. Evaluation of the performance of different atmospheric chemical transport models and inter-comparison of nitrogen and sulphur deposition estimates for the UK. Atmos. Environ. 119, 131–143. https://doi.org/10.1016/j.atmosenv.2015.08.008.

Draxler, R., Arnold, D., Chino, M., Galmarini, S., Hort, M., Jones, A., Leadbetter, S., Malo, A., Maurer, C., Rolph, G., Saito, K., Servranckx, R., Shimbori, T., Solazzo, E., Wotawa, G., 2015. World Meteorological Organization's model simulations of the radionuclide dispersion and deposition from the Fukushima Daiichi nuclear power plant accident. J. Environ. Radioact. 139, 172–184. https://doi.org/10.1016/j.jenvrad.2013.09.014.

Eyring, V., Bony, S., Meehl, G.A., Senior, C.A., Stevens, B., Stouffer, R.J., Taylor, K.E., 2016. Overview of the coupled model intercomparison project phase 6 (CMIP6) experimental design and organization. Geosci. Model Dev. (GMD) 9, 1937–1958. https://doi.org/10.5194/gmd-9-1937-2016.

Frehlich, R., Sharman, R., 2008. The use of structure functions and spectra from numerical model output to determine effective model resolution. Mon. Weather Rev. 136, 1537–1553. https://doi.org/10.1175/2007MWR2250.1.

Goto, D., Morino, Y., Ohara, T., Sekiyama, T.T., Uchida, J., Nakajima, T., 2020. Application of linear minimum variance estimation to the multi-model ensemble of atmospheric radioactive Cs-137 with observations. Atmos. Chem. Phys. 20, 3589–3607. https://doi.org/10.5194/acp-20-3589-2020.

Graziani, G., Galmarini, S., Grippa, G., Klug, W., 1998. Real-time Long-Range Dispersion Model Evaluation of the ETEX [European Tracer Experiment]. Second Release, European Union.

Grell, G.A., Peckham, S.E., Schmitz, R., McKeen, S.A., Frost, G., Skamarock, W.C., Eder, B., 2005. Fully coupled "online" chemistry within the WRF model. Atmos. Environ. 39, 6957–6975. https://doi.org/10.1016/j.atmosenv.2005.04.027.

Honda, M.C., Aono, T., Aoyama, M., Hamajima, Y., Kawakami, H., Kitamura, M., Masumoto, Y., Miyazawa, Y., Takigawa, M., Saino, T., 2012. Dispersion of artificial caesium-134 and -137 in the western North Pacific one month after the Fukushima accident. Geochem. J. 46, e1–e9. https://doi.org/10.2343/geochemj.1.0152.

Hu, X., Li, D., Huang, H., Shen, S., Bou-Zeid, E., 2014. Modeling and sensitivity analysis of transport and deposition of radionuclides from the Fukushima Dai-ichi accident. Atmos. Chem. Phys. 14, 11065–11092. https://doi.org/10.5194/acp-14-11065-2014.

Huneeus, N., Schulz, M., Balkanski, Y., Griesfeller, J., Prospero, J., Kinne, S., Bauer, S., Boucher, O., Chin, M., Dentener, F., Diehl, T., Easter, R., Fillmore, D., Ghan, S., Ginoux, P., Grini, a., Horowitz, L., Koch, D., Krol, M.C., Landing, W., Liu, X., Mahowald, N., Miller, R., Morcrette, J.J., Myhre, G., Penner, J., Perlwitz, J., Stier, P., Takemura, T., Zender, C.S., 2011. Global dust model intercomparison in AeroCom phase i. Atmos. Chem. Phys. 11, 7781–7816. https://doi.org/10.5194/acp-11-7781-2011.

Igarashi, Y., Kajino, M., Zaizen, Y., Adachi, K., Mikami, M., 2015. Atmospheric radioactivity over Tsukuba, Japan: a summary of three years of observations after the FDNPP accident. Prog. Earth Planet Sci. 2, 44. https://doi.org/10.1186/s40645-015-0066-1.

Institute for Global Environment and Society (IGES), 1989. Grid analysis and Display system (GrADS). http://www.iges.org/grads/grads.html accessed 5.1.14.

Kajino, M., Deushi, M., Sekiyama, T.T., Oshima, N., Yumimoto, K., Tanaka, T.Y., Ching, J., Hashimoto, A., Yamamoto, T., Ikegami, M., Kamada, A., Miyashita, M., Inomata, Y., Shima, S.I., Takami, A., Shimizu, A., Hatakeyama, S., 2019a. NHM-Chem, the Japan meteorological agency's regional meteorology – chemistry model: model evaluations toward the consistent predictions of the chemical, physical, and optical properties of aerosols. J. Meteorol. Soc. Jpn. 97, 337–374. https://doi.org/10.2151/JMSJ.2019-020.

Kajino, M., Ishizuka, M., Igarashi, Y., Kita, K., Yoshikawa, C., Inatsu, M., 2016. Long-term assessment of airborne radiocesium after the Fukushima nuclear accident: Re-suspension from bare soil and forest ecosystems. Atmos. Chem. Phys. 16, 13149–13172. https://doi.org/10.5194/acp-16-13149-2016.

Kajino, M., Sekiyama, T.T., Igarashi, Y., Katata, G., Sawada, M., Adachi, K., Zaizen, Y., Tsuruta, H., Nakajima, T., 2019b. Deposition and dispersion of radio-cesium released due to the Fukushima Nuclear accident: sensitivity to meteorological models and physical modules. J. Geophys. Res. Atmos. 124, 1823–1845. https://doi.org/10.1029/2018JD028998.

Kaneyasu, N., Ohashi, H., Suzuki, F., Okuda, T., Ikemori, F., 2012. Sulfate aerosol as a potential transport medium of radiocesium from the Fukushima Nuclear Accident. Environ. Sci. Technol. 46, 5720–5726. https://doi.org/10.1021/es204667h.

Katata, G., Chino, M., Kobayashi, T., Terada, H., Ota, M., Nagai, H., Kajino, M., Draxler, R., Hort, M.C., Malo, A., Torii, T., Sanada, Y., 2015. Detailed source term estimation of the atmospheric release for the Fukushima Daiichi Nuclear Power Station accident by coupling simulations of an atmospheric dispersion model with an improved deposition scheme and oceanic dispersion model. Atmos. Chem. Phys. 15, 1029–1070. https://doi.org/10.5194/acp-15-1029-2015.

Katata, G., Ota, M., Terada, H., Chino, M., Nagai, H., 2012. Atmospheric discharge and dispersion of radionuclides during the Fukushima Dai-ichi Nuclear Power Plant accident. Part I: source term estimation and local-scale atmospheric dispersion in

early phase of the accident. J. Environ. Radioact. 109, 103–113. https://doi.org/10.1016/j.jenvrad.2012.02.006.
Kitayama, K., Morino, Y., Takigawa, M., Nakajima, T., Hayami, H., Nagai, H., Terada, H., Saito, K., Shimbori, T., Kajino, M., Sekiyama, T.T., Didier, D., Mathieu, A., Quélo, D., Ohara, T., Tsuruta, H., Oura, Y., Ebihara, M., Moriguchi, Y., Shibata, T., 2018. Atmospheric modeling of 137 Cs plumes from the Fukushima Daiichi Nuclear Power Plant-evaluation of the model intercomparison data of the science council of Japan. J. Geophys. Res. Atmos. 123 https://doi.org/10.1029/2017JD028230.
Kondo, H., Saigusa, N., Murayama, S., Yamamoto, S., Kannari, A., 2001. A numerical simulation of the daily variation of CO2 in the central part of Japan-summer case. J. Meteorol. Soc. Jpn. 79, 11–21. https://doi.org/10.2151/jmsj.79.11.
Korsakissok, I., Mathieu, A., Didier, D., 2013. Atmospheric dispersion and ground deposition induced by the Fukushima Nuclear Power Plant accident: a local-scale simulation and sensitivity study. Atmos. Environ. 70, 267–279. https://doi.org/10.1016/j.atmosenv.2013.01.002.
Leadbetter, S.J., Hort, M.C., Jones, A.R., Webster, H.N., Draxler, R.R., 2015. Sensitivity of the modelled deposition of Caesium-137 from the Fukushima Dai-ichi nuclear power plant to the wet deposition parameterisation in NAME. J. Environ. Radioact. 139, 200–211. https://doi.org/10.1016/j.jenvrad.2014.03.018.
Li, X., Sun, S., Hu, X., Huang, H., Li, H., Morino, Y., Wang, S., Yang, X., Shi, J., Fang, S., 2019. Source inversion of both long- and short-lived radionuclide releases from the Fukushima Daiichi nuclear accident using on-site gamma dose rates. J. Hazard Mater. 379, 120770. https://doi.org/10.1016/j.jhazmat.2019.120770.
Maki, T., 2015. Emission source estimation by an inverse model, in: contribution of JMA to the WMO technical task team on meteorological analyses for Fukushima Daiichi Nuclear Power Plant accident and relevant atmospheric transport modelling at MRI (in Japanese). In: Tech. Tsukuba.
Mathieu, A., Kajino, M., Korsakissok, I., Périllat, R., Quélo, D., Quérel, A., Saunier, O., Sekiyama, T.T., Igarashi, Y., Didier, D., 2018. Fukushima Daiichi–derived radionuclides in the atmosphere, transport and deposition in Japan: a review. Appl. Geochem. 91, 122–139. https://doi.org/10.1016/j.apgeochem.2018.01.002.
Mathieu, A., Korsakissok, I., Quelo, D., Groell, J., Tombette, M., Didier, D., Quentric, E., Saunier, O., Benoit, J.-P., Isnard, O., 2012. Atmospheric dispersion and deposition of radionuclides from the Fukushima Daiichi nuclear power plant accident. Elements 8, 195–200. https://doi.org/10.2113/gselements.8.3.195.
Meehl, G.A., Boer, G.J., Covey, C., Latif, M., Stouffer, R.J., 2000. The coupled model intercomparison project (CMIP). Bull. Am. Meteorol. Soc. 81, 313–318. https://doi.org/10.1175/1520-0477(2000)081<0313:TCMIPC>2.3.CO;2.
Japanese Ministry of Education, Culture, Sports, Science and Technology (MEXT), 2011. Results of the fourth airborne monitoring survey by MEXT. http://radioactivity.nsr.go.jp/en/contents/4000/3179/24/1270_1216.pdf. (Accessed 11 August 2020).
Moriizumi, J., Oku, A., Yaguchi, N., Kuwahara, Y., Yamazawa, H., 2019. Spatial distributions of atmospheric concentrations of radionuclides on 15 March 2011 discharged by the Fukushima Dai-Ichi Nuclear Power Plant Accident estimated from NaI(Tl) pulse height distributions measured in Ibaraki Prefecture. J. Nucl. Sci. Technol. 1–19. https://doi.org/10.1080/00223131.2019.1699191.
Morino, Y., Ohara, T., Nishizawa, M., 2011. Atmospheric behavior, deposition, and budget of radioactive materials from the Fukushima Daiichi nuclear power plant in March 2011. Geophys. Res. Lett. 38 https://doi.org/10.1029/2011GL048689.
Morino, Y., Ohara, T., Watanabe, M., Hayashi, S., Nishizawa, M., 2013. Episode analysis of deposition of radiocesium from the Fukushima Daiichi nuclear power plant accident. Environ. Sci. Technol. 47, 2314–2322. https://doi.org/10.1021/es304620x.
Myhre, G., Samset, B.H., Schulz, M., Balkanski, Y., Bauer, S., Berntsen, T.K., Bian, H., Bellouin, N., Chin, M., Diehl, T., Easter, R.C., Feichter, J., Ghan, S.J., Hauglustaine, D., Iversen, T., Kinne, S., Kirkevåg, A., Lamarque, J.-F., Lin, G., Liu, X., Lund, M.T., Luo, G., Ma, X., van Noije, T., Penner, J.E., Rasch, P.J., Ruiz, A., Seland, Ø., Skeie, R.B., Stier, P., Takemura, T., Tsigaridis, K., Wang, P., Wang, Z., Xu, L., Yu, H., Yu, F., Yoon, J.-H., Zhang, K., Zhang, H., Zhou, C., 2013. Radiative forcing of the direct aerosol effect from AeroCom Phase II simulations. Atmos. Chem. Phys. 13, 1853–1877. https://doi.org/10.5194/acp-13-1853-2013.
Nakajima, T., Misawa, S., Morino, Y., Tsuruta, H., Goto, D., Uchida, J., Takemura, T., Ohara, T., Oura, Y., Ebihara, M., Satoh, M., 2017. Model depiction of the atmospheric flows of radioactive cesium emitted from the Fukushima Daiichi Nuclear Power Station accident. Prog. Earth Planet Sci. 4, 2. https://doi.org/10.1186/s40645-017-0117-x.
Nishizawa, S., Yashiro, H., Sato, Y., Miyamoto, Y., Tomita, H., 2015. Influence of grid aspect ratio on planetary boundary layer turbulence in large-eddy simulations. Geosci. Model Dev. (GMD) 8, 3393–3419. https://doi.org/10.5194/gmd-8-3393-2015.
Oura, Y., Ebihara, M., Tsuruta, H., Nakajima, T., Ohara, T., Ishimoto, M., Sawahata, H., Katsumura, Y., Nitta, W., 2015. A database of hourly atmospheric concentrations of radiocesium (^{134}Cs and ^{137}Cs) in suspended particulate matter collected in March 2011 at 99 air pollution monitoring stations in eastern Japan. J. Nucl. Radiochem. Sci. 15, 2_1–2_12. https://doi.org/10.14494/jnrs.15.2_1.
Quérel, A., Roustan, Y., Quélo, D., Benoit, J.P., 2015. Hints to discriminate the choice of wet deposition models applied to an accidental radioactive release. Int. J. Environ. Pollut. 58, 268. https://doi.org/10.1504/IJEP.2015.077457.
Saito, K., Shimbori, T., Draxler, R., 2015. JMA's regional atmospheric transport model calculations for the WMO technical task team on meteorological analyses for Fukushima Daiichi Nuclear Power Plant accident. J. Environ. Radioact. 139, 185–199. https://doi.org/10.1016/j.jenvrad.2014.02.007.
Sanada, Y., Katata, G., Kaneyasu, N., Nakanishi, C., Urabe, Y., Nishizawa, Y., 2018. Altitudinal characteristics of atmospheric deposition of aerosols in mountainous regions: lessons from the Fukushima Daiichi Nuclear Power Station accident. Sci. Total Environ. 618, 881–890. https://doi.org/10.1016/j.scitotenv.2017.08.246.
Sato, Y., Nishizawa, S., Yashiro, H., Miyamoto, Y., Kajikawa, Y., Tomita, H., 2015. Impacts of cloud microphysics on trade wind cumulus: which cloud microphysics processes contribute to the diversity in a large eddy simulation? Prog. Earth Planet Sci. 2, 23. https://doi.org/10.1186/s40645-015-0053-6.
Sato, Y., Takigawa, M., Sekiyama, T.T., Kajino, M., Terada, H., Nagai, H., Kondo, H., Uchida, J., Goto, D., Quélo, D., Mathieu, A., Quérel, A., Fang, S., Morino, Y., von Schoenberg, P., Grahn, H., Brännström, N., Hirao, S., Tsuruta, H., Yamazawa, H., Nakajima, T., 2018. Model intercomparison of atmospheric 137 Cs from the Fukushima Daiichi Nuclear Power Plant Accident: simulations based on identical input data. J. Geophys. Res. Atmos. 123, 1–18. https://doi.org/10.1029/2018JD029144.
Satoh, M., Tomita, H., Yashiro, H., Miura, H., Kodama, C., Seiki, T., Noda, A.T., Yamada, Y., Goto, D., Sawada, M., Miyoshi, T., Niwa, Y., Hara, M., Ohno, T., Iga, S., Arakawa, T., Inoue, T., Kubokawa, H., 2014. The non-hydrostatic icosahedral atmospheric model: description and development. Prog. Earth Planet Sci. 1, 18. https://doi.org/10.1186/s40645-014-0018-1.
Saunier, O., Mathieu, A., Didier, D., Tombette, M., Quélo, D., Winiarek, V., Bocquet, M., 2013. An inverse modeling method to assess the source term of the Fukushima Nuclear Power Plant accident using gamma dose rate observations. Atmos. Chem. Phys. 13, 11403–11421. https://doi.org/10.5194/acp-13-11403-2013.
Science Council of Japan, 2014. A Review of the Model Comparison of Transportation and Deposition of Radioactive Materials Released to the Environment as a Result of the Tokyo Electric Power Company's Fukushima Daiichi Nuclear Power Plant Accident. Tokyo.
Sekiyama, T.T., Kajino, M., 2020. Reproducibility of surface wind and tracer Transport simulations over complex terrain using 5-, 3-, and 1-km-grid models. J. Appl. Meteorol. Climatol. 59, 937–952. https://doi.org/10.1175/JAMC-D-19-0241.1.
Sekiyama, T.T., Kajino, M., Kunii, M., 2017. The impact of surface wind data assimilation on the predictability of near-surface plume advection in the case of the Fukushima Nuclear Accident. J. Meteorol. Soc. Jpn. Ser. II 95, 447–454. https://doi.org/10.2151/jmsj.2017-025.
Sekiyama, T.T., Kunii, M., Kajino, M., Shimbori, T., 2015. Horizontal resolution dependence of atmospheric simulations of the Fukushima Nuclear Accident Using 15-km, 3-km, and 500-m grid models. J. Meteorol. Soc. Jpn. Ser. II 93, 49–64. https://doi.org/10.2151/jmsj.2015-002.
Skamarock, W.C., 2004. Evaluating mesoscale NWP models using kinetic energy spectra. Mon. Weather Rev. 132, 3019–3032. https://doi.org/10.1175/MWR2830.1.
Stevens, B., Moeng, C.-H., Ackerman, A.S., Bretherton, C.S., Chlond, A., de Roode, S., Edwards, J., Golaz, J.-C., Jiang, H., Khairoutdinov, M., Kirkpatrick, M.P., Lewellen, D.C., Lock, A., Müller, F., Stevens, D.E., Whelan, E., Zhu, P., 2005. Evaluation of large-eddy simulations via observations of nocturnal marine stratocumulus. Mon. Weather Rev. 133, 1443–1462. https://doi.org/10.1175/MWR2930.1.
Stohl, A., Seibert, P., Wotawa, G., Arnold, D., Burkhart, J.F., Eckhardt, S., Tapia, C., Vargas, A., Yasunari, T.J., 2012. Xenon-133 and caesium-137 releases into the atmosphere from the Fukushima Dai-ichi nuclear power plant: determination of the source term, atmospheric dispersion, and deposition. Atmos. Chem. Phys. 12, 2313–2343. https://doi.org/10.5194/acp-12-2313-2012.
Takemura, T., Nakamura, H., Takigawa, M., Kondo, H., Satomura, T., Miyasaka, T., Nakajima, T., 2011. A numerical simulation of global transport of atmospheric particles emitted from the Fukushima Daiichi Nuclear Power Plant. SOLA 7, 101–104. https://doi.org/10.2151/sola.2011-026.
Taylor, K.E., 2001. Summarizing multiple aspects of model performance in a single diagram. J. Geophys. Res. Atmos. 106, 7183–7192. https://doi.org/10.1029/2000JD900719.
Terada, H., Katata, G., Chino, M., Nagai, H., 2012. Atmospheric discharge and dispersion of radionuclides during the Fukushima Dai-ichi Nuclear Power Plant accident. Part II: verification of the source term and analysis of regional-scale atmospheric dispersion. J. Environ. Radioact. 112, 141–154. https://doi.org/10.1016/j.jenvrad.2012.05.023.
Terada, H., Nagai, H., Tsuduki, K., Furuno, A., Kadowaki, M., Kakefuda, T., 2020. Refinement of source term and atmospheric dispersion simulations of radionuclides during the Fukushima Daiichi Nuclear Power Station accident. J. Environ. Radioact. 213, 106104. https://doi.org/10.1016/j.jenvrad.2019.106104.
Terasaka, Y., Yamazawa, H., Hirouchi, J., Hirao, S., Sugiura, H., Moriizumi, J., Kuwahara, Y., 2016. Air concentration estimation of radionuclides discharged from Fukushima Daiichi Nuclear Power Station using NaI(Tl) detector pulse height distribution measured in Ibaraki Prefecture. J. Nucl. Sci. Technol. 53, 1919–1932. https://doi.org/10.1080/00223131.2016.1193453.
Thibeault, J.M., Seth, a., Garcia, M., 2010. Changing climate in the Bolivian Altiplano: CMIP3 projections for temperature and precipitation extremes. J. Geophys. Res. 115, D08103. https://doi.org/10.1029/2009JD012718.
Tsuruta, H., Oura, Y., Ebihara, M., Moriguchi, Y., Ohara, T., Nakajima, T., 2018. Time-series analysis of atmospheric radiocesium at two SPM monitoring sites near the Fukushima Daiichi Nuclear Power Plant just after the Fukushima accident on March 11, 2011. Geochem. J. 52, 103–121. https://doi.org/10.2343/geochemj.2.0520.
Tsuruta, H., Oura, Y., Ebihara, M., Ohara, T., Nakajima, T., 2014. First retrieval of hourly atmospheric radionuclides just after the Fukushima accident by analyzing filter-tapes of operational air pollution monitoring stations. Sci. Rep. 4, 6717. https://doi.org/10.1038/srep06717.
Uchida, J., Mori, M., Hara, M., Satoh, M., Goto, D., Kataoka, T., Suzuki, K., Nakajima, T., 2017. Impact of lateral boundary errors on the simulation of clouds with a nonhydrostatic regional climate model. Mon. Weather Rev. 145, 5059–5082. https://doi.org/10.1175/MWR-D-17-0158.1.
VanZanten, M.C., Stevens, B., Nuijens, L., Siebesma, A.P., Ackerman, A.S., Burnet, F., Cheng, A., Couvreux, F., Jiang, H., Khairoutdinov, M., Kogan, Y., Lewellen, D.C.,

Mechem, D., Nakamura, K., Noda, A., Shipway, B.J., Slawinska, J., Wang, S., Wyszogrodzki, A., 2011. Controls on precipitation and cloudiness in simulations of trade-wind cumulus as observed during RICO. J. Adv. Model. Earth Syst. 3, M06001. https://doi.org/10.1029/2011MS000056.

Wang, Z., Huang, X., Ding, A., 2019. Optimization of vertical grid setting for air quality modelling in China considering the effect of aerosol-boundary layer interaction. Atmos. Environ. 210, 1–13. https://doi.org/10.1016/j.atmosenv.2019.04.042.

Yasunari, T.J., Stohl, A., Hayano, R.S., Burkhart, J.F., Eckhardt, S., Yasunari, T., 2011. Cesium-137 deposition and contamination of Japanese soils due to the Fukushima nuclear accident. Proc. Natl. Acad. Sci. 108, 19530–19534. https://doi.org/10.1073/pnas.1112058108.